DESIGN OF CEBAF's RF SEPARATOR AND RESULTS OF COLD TESTS

C. G. Yao

Continuous Electron Beam Accelerator Facility
12000 Jefferson Avenue
Newport News, Virginia 23606

Abstract

The design of the CEBAF accelerator system is based upon a multipass racetrack configuration, the straight sections of which will utilize 1497-MHz superconducting linac sections with independent magnetic transport at the end of each linac segment. Room-temperature SW rf separators operating at a frequency of 998 MHz will be used in each independent transport channel at one end of the racetrack to extract a portion of the recirculating current. With the frequency chosen and appropriate phasing, three independent beams of correlated energy may be extracted for use in the three experimental areas. The design of the rf separators, based on an alternating periodic structure (APS), will be described and some preliminary prototype cold test results will be given.

Introduction

The CEBAF accelerator will serve three experimental stations simultaneously. Five rf separators and their supportive beam optics systems will be used to extract the required beam. By appropriate phasing of the rf separator system the beam may be split into either two or three separate beams (see Figure 1). In order to meet this particular requirement, the choice of the operating frequency for the rf separator is not arbitrary. Let f_1 be the bunch frequency and f_2 be the frequency of the deflecting wave. Suppose the first bunch enters the separator at phase θ; subsequent bunches will then enter the separator at phases $\theta + 2\pi f_2/f_1, \theta + 4\pi f_2/f_1 \ldots, \theta + n\ 2\pi\ f_2/f_1$. Since the fourth bunch has the same phase as the first and the second bunch does not, a relationship can be obtained between f_1 and f_2:

$$f_2 = \frac{mf_1}{3} \tag{1}$$

where m is an integer not divisible by 3.

The primary accelerating frequency chosen for CEBAF is 1497 MHz. Therefore, frequencies of 499 MHz, 998 MHz, 1996 MHz, and 2495 MHz would be appropriate for the rf separator. The lowest frequency, 499 MHz, was eliminated because the size of the deflecting structure would be too large (only 50 cm is available between beamlines). Higher frequencies cause dilution of the transverse emittance, thus making lower frequencies preferable. The operating frequency chosen for the rf separators is 998 MHz.

The HEM_{11} wave is used for deflecting micro-bunches in the rf separators because it affords uniformity of deflection independent of the transverse position of electrons in the central region of the structure. A transverse momentum $p_\perp$ imparted to an electron moving through a separator of length L on the crest of the deflecting wave is given by

$$p_\perp = \frac{e}{c}\sqrt{R_\perp P_L L} \tag{2}$$

where $R_\perp$ is the transverse shunt impedance of per unit length of the structure and P_L is the input power to the structure.

Structure Design

Most rf separators which were built at CERN,[1] SLAC,[2,3] and BNL[4,5] are uniform disk-loaded waveguide structures that operate at high pulse power and with a traveling wave mode of $\pi/2$ or $2\pi/3$. The deflecting angle required for these applications, particle separation, is about 1 mrad.

CEBAF's rf separators run at room temperature with continuous waves. The deflecting angle required to split beams is only $\approx$ 0.10 mrad. In addition, there is a restriction on the space along the beamline available for the rf separators. Based on these requirements,[6] the standing wave mode was selected.

Biperiodic Structures

The maximum deflection in standing structures is achieved by operating in the π mode. However, the π mode is the most sensitive to frequency errors. In contrast, the $\frac{\pi}{2}$ mode structure is the least sensitive. However, the transverse shunt impedance is substantially lower because of the absence of field in every other cavity of the structure. Biperiodic structures in which the unexcited cavities are shortened or put off the axis are a reasonable compromise between stability and efficiency.

For the biperiodic structures, the dispersion equation is

$$k_0^2\cos^2\phi = \left[1 - \left(\frac{f_a}{f}\right)^2 + k_1\cos 2\phi\right] \times \left[1 - \left(\frac{f_c}{f}\right)^2 + k_2\cos 2\phi\right] \tag{3}$$

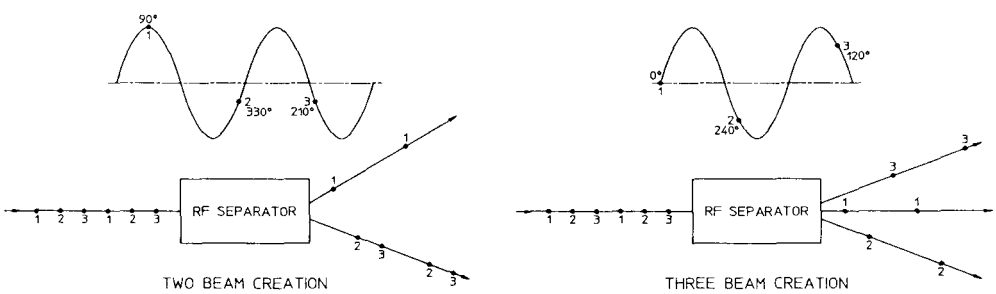

Figure 1 Two operation states of CEBAF's rf separators.

where f_a and f_c are the coherent frequencies of the deflecting and coupling cavities, respectively; k_0 is the coupling coefficient between deflecting and adjacent coupling cavities; k_1 is the direct coupling coefficient between deflecting cavities; and k_2 is the direct coupling coefficient between coupling cavities. For the $\frac{\pi}{2}$ mode ($\phi = \frac{\pi}{2}$) the dispersion equation (3) becomes the two independent equations that give two frequencies for the $\frac{\pi}{2}$ modes as follows:

$$(f_{\frac{\pi}{2}})_a = \frac{f_a}{\sqrt{1-k_1}} \tag{4}$$

$$(f_{\frac{\pi}{2}})_c = \frac{f_c}{\sqrt{1-k_2}}. \tag{5}$$

They correspond to two kinds of field distribution in the structure. A condition for confluence at the operating frequency f_0 or

$$(f_{\frac{\pi}{2}})_a = (f_{\frac{\pi}{2}})_c = f_0$$

is

$$\frac{f_a}{f_c} = \frac{\sqrt{1-k_1}}{\sqrt{1-k_2}}. \tag{6}$$

Stop bandwidth df is

$$df = (f_{\frac{\pi}{2}})_a - (f_{\frac{\pi}{2}})_c.$$

To achieve a stable biperiodic structure it is important to keep df as close to zero as possible. Two kinds of biperiodic structures are discussed below.

Alternating Periodic Structure

Shortening the unexcited cavities and lengthening the excited cavities correspondingly in a disk-loaded waveguide (see Figure 2) lead to the alternating periodic structure (APS). Figure 3 shows a relationship of $R_\perp/Q$ vs a/λ for an APS. The curve is flat when a/λ is small and gradually decreases as a/λ increases. The value of $R_\perp/Q$ in the APS is very close to that of the π mode in the single periodic structure if the length of the coupling cavity is relatively short, e.g., 15–20 mm at a frequency of 1 GHz. However, the APS has much greater stability than the simple periodic structure of π mode.

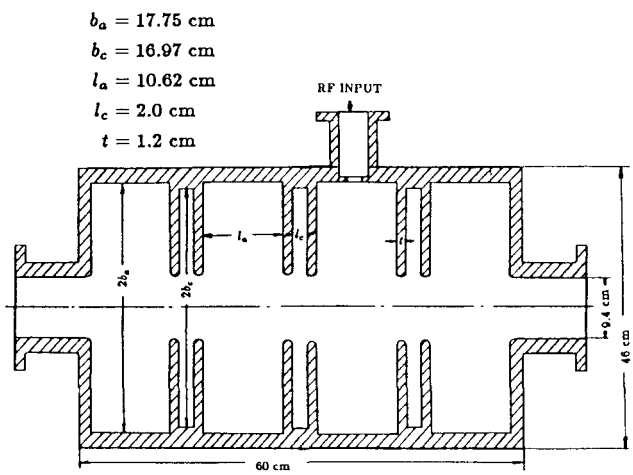

Figure 2

Preliminary design of CEBAF's rf separator at first channel.

Calculations using the computer code URMEL show some useful results:

1. As thickness t of the disks decreases, the transverse shunt impedance $R_\perp$ increases and the passband expands, but the capacity for heat transfer and structure rigidity lessens.
2. There is an optimum aperture radius a that makes the passband widest for a certain l_c, the length of the coupling cavity and a certain t.
3. As l_c increases, the maximum passband width increases, but $R_\perp$ decreases.

The final selection of the structure dimensions will be a compromise among many factors, e. g., heat transfer, structure rigidity, frequency sensitivity, passband width/group velocity, and transverse shunt impedance. Table 1 gives the parameters of the APS which are presently selected for CEBAF's rf separators as shown in Figure 2.

Table 1
Parameters of APS for CEBAF's RF Separators

Frequency f	998 MHz
Wavelength λ	30.0393 cm
Mode ϕ	$\pi/2$
Group velocity v_g/c	-0.024
Aperture radius a	4.7 cm (round edge)
Disk thickness t	1.2 cm
Coupling cell length l_c	2.0 cm
Deflecting cell length l_a	10.62 cm
Coupling cell diameter $2b_c$	33.852 cm
Deflecting cell diameter $2b_a$	35.397 cm
End cell diameter $2b_e$	35.64 cm
$R_\perp/Q$	502 Ω/m
Q of the deflecting cavity	31400
Q of the coupling cavity	9200
Power consumption	63.4 kW/m (at $E_\perp$ = 1 MeV/m)

It can be seen from Table 1 that b_c is smaller than b_a for confluence in an APS working at dipole mode.[7] This shows the difference in property of HEM_{11} mode from that of TM_{01} mode. In an accelerating APS,[8] the b_c is larger than b_a for the

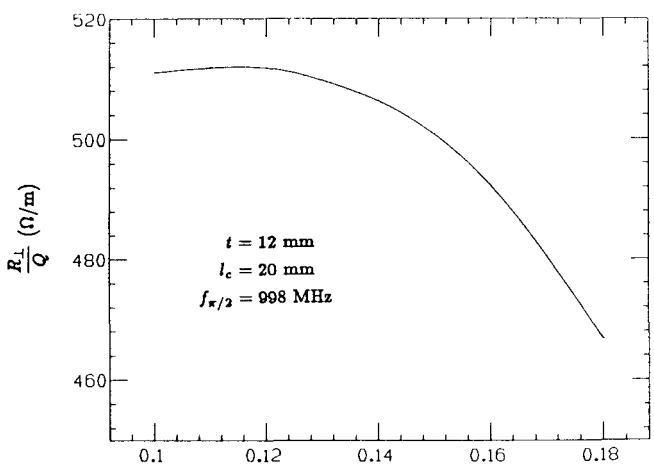

Figure 3 $R_\perp/Q$ vs a/λ for an APS structure.

confluence. The calculations show that the end deflecting cell radius b_e should be larger than regular deflecting cell radius b_a for the confluence at $\pi/2$ mode; this leads to a lower field in the end cell than that in the regular cell.

Figure 4 gives b_a and b_c for the confluence at the $\pi/2$ mode as a/λ changes. Figure 5 gives the various Q_a and Q_c as a/λ changes. Figure 6 gives $\frac{\partial f_a}{\partial b_a}$, $\frac{\partial f_c}{\partial b_c}$, $\frac{\partial f_a}{\partial a}$, and $\frac{\partial f_c}{\partial a}$ again as a/λ changes; all of these derivatives are negative. They are useful in determining tolerances on the different dimensions and in selecting methods to tune up the structure.

There is another particular cavity, the input cavity, that is directly connected to an rf input waveguide. The radius of this cavity is b_{in}. The dimensions b_a, b_e, b_{in} and b_c must be finally determined by experiments.

The entire rf separator system consists of five rf separators. Table 2 shows the major parameters for each of them based on the APS design mentioned above. The relative momentum kick requirement is 10^{-4}. The last column gives the estimated source power requirements, which are 50% higher than the calculated values to include transmission losses, actual conditions of material and machining, coupling losses, and a contingency. The design of the optical system requires that the first four rf separators operate in a "two-beam state" during which the kicked beam is located on the crest of the wave. The rf separator for the highest energy runs in a "three-beam state" with the kicked beams phased at 60°. This means that the deflecting field should be about 16% higher than that expected when beams are at the crest.

Table 2
Power Requirements

Beam-Line	Length (cm)	Energy (GeV)	Kick Momentum ($\frac{keV}{c}$)	Power Consumption (kW)	Source Power (kW)
1	60	1.2	120	1.6	2.4
2	120	2.4	240	3.1	4.7
3	120	3.6	360	6.9	10.4
4	210	4.8	480	7.0	10.5
5	2 × 120	6.0	600	12.6	18.9

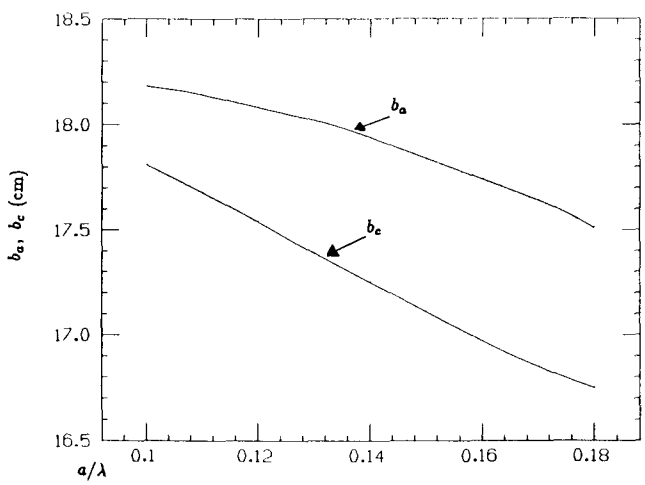

Figure 4 b_a and b_c for confluence at $\pi/2$ mode vs a/λ.

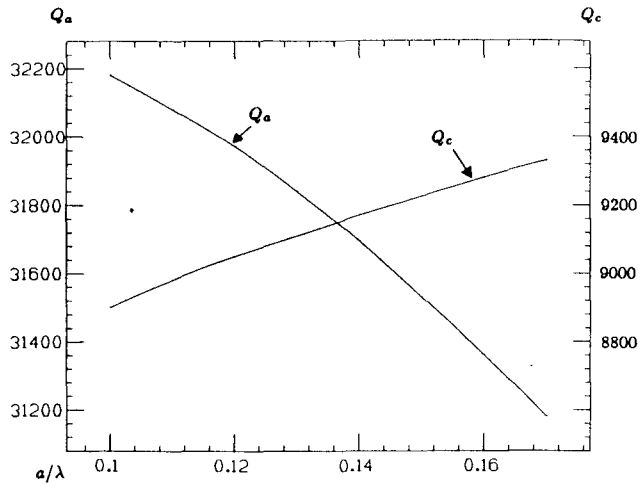

Figure 5 Q_a and Q_c vs a/λ.

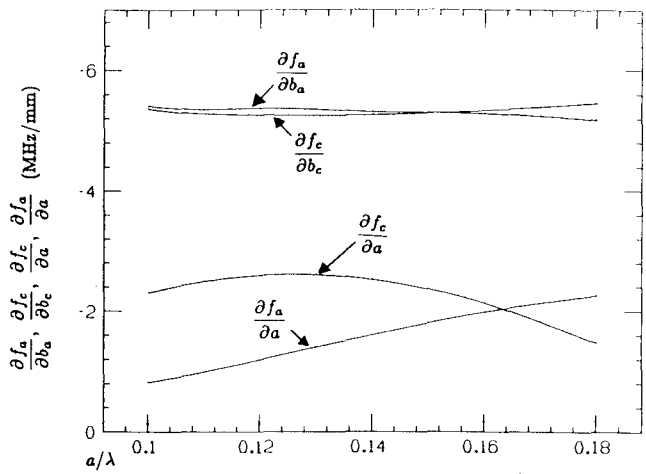

Figure 6 Derivatives of frequency with respect to cavity dimensions as a/λ changes.

SCS and OCS

Performances of shaped cavities with nose cones that constitute the deflecting units in side-coupled structures (SCS) and on-axis coupled structures (OCS) were calculated.

The SCS is more complicated to manufacture than the OCS, but it has higher $R_\perp/Q$ than OCS, at least theoretically.

Calculations using URMEL indicate that the SCS or OCS can achieve about 40% higher $R_\perp$ than that of APS or π mode for single periodic structures. This is the major advantage of SCS or OCS. In addition, the calculations show that the deflecting field is uniform in the central region of cavities with nose cones.

Mode Degeneration

Mode degeneration is a particular problem that occurs in an rf separator structure. A mode rotation, or a rotation in the polarization direction of the dipole mode, is very likely to happen in a cylindrical structure. It causes a rotation of the deflecting beam. We want to deflect the beam on a horizontal plane, and therefore, the direction at which the beam is deflected must be stabilized.

There are several techniques for mode stabilization: flat parts in the cavity shape, used at CERN; a bar pair close to the cavity wall in the axial direction, used at BNL; or holes through the disks,[9] used at SLAC. We decided to use a bar pair as a mode stabilizer because of its simplicity to manufacture. In addition, the bars in the proper position have little effect on the frequency of the mode which has polarization in the deflecting direction.

Results of Cold Tests

A basic experimental model was designed and fabricated for cold tests on CEBAF's rf separators (APS) shown in Figure 7. The test set, composed of one deflecting cell and two coupling half-cells, was excited by antennae. The fields were strong in the two end half-cells and almost empty in the central cell for $\pi/2$ mode because of the means of exciting the cavity set. A relationship between $(f_{\frac{\pi}{2}})_c$ and $2b_c$, the diameter of the coupling cell, was obtained by changing two half-end-cells and measuring the frequency of $\pi/2$ mode. Figure 8 shows these relationships. Curve 1 is the experimental one, and curve 2 was calculated by URMEL. If we use a coupling cell in the central region and two half-deflecting-cells in the two ends and perform the same measurements, another set of curves is obtained (shown in Figure 9) which corresponds to $(f_{\frac{\pi}{2}})_a$ and $2b_a$. All measurements were made at 78°F, and a vacuum correction of 0.3 MHz was taken into account. It can be seen from the figures that $(2b_a)_{exp} = 35.398$ cm and $(2b_a)_{cal} = 35.397$ cm, and that $(2b_c)_{exp} = 33.876$ cm and $(2b_c)_{cal} = 33.852$ cm (they are compatible). The greater error in b_c comes from the fact that the coupling holes on the end plates and the antennae have a larger effect on the frequencies of the shorter coupling half-cells.

In order to determine the frequency split caused by the bars, we put several different sizes of bar pairs through the entire test set, from one end plate to another, in both sides of the cell center but a distance R_b away from the center. The line connecting the centers of the bars passes through the center of the cell. By measuring the frequencies of the modes in two directions perpendicular to each other, of which one has a polar direction parallel to the connecting line of the bars (unwanted mode) and another has a polar direction perpendicular to the former one (operating mode), we can determine the frequency shifts of the unwanted mode caused by the bar pair and the effects of the bar pair on the frequency of the operating mode. The results of these experiments are shown in Figure 10. The experimental data are in agreement with those computed by MAFIA.[10] Based on the data, we are able to determine the size of the bars and their location as the mode stabilizer.

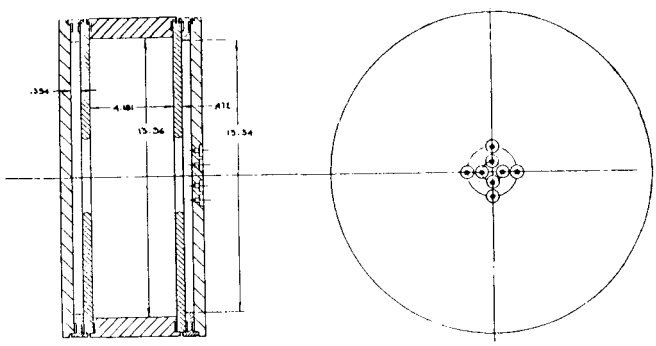

Figure 7 Scheme of cold test set for determination of APS dimension 2*b*.

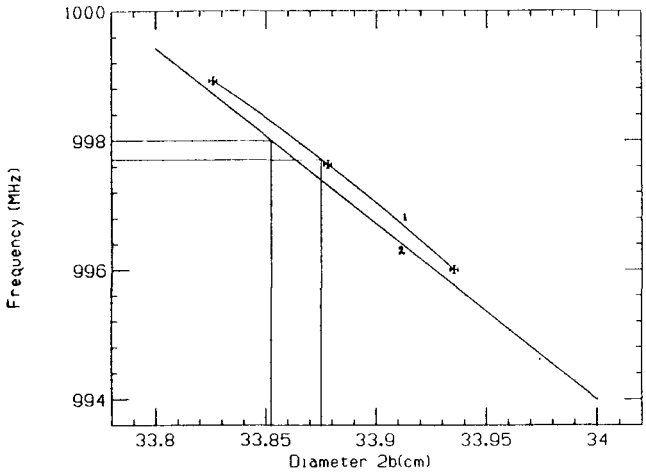

Figure 8 $(f_{\pi/2})_c$ vs dimension of coupling cell.

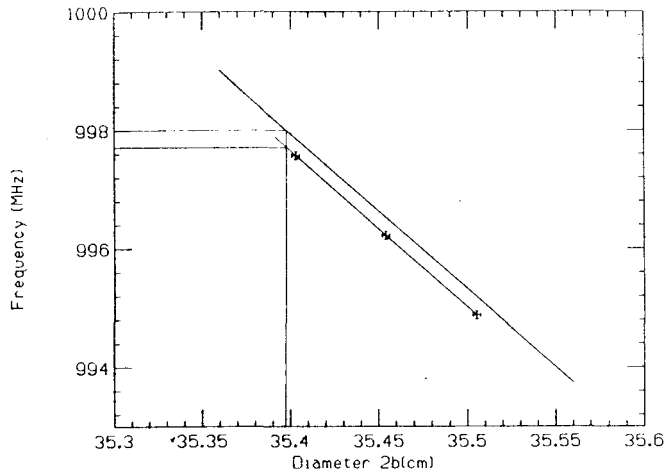

Figure 9 $(f_{\pi/2})_a$ vs dimension of deflecting cell.

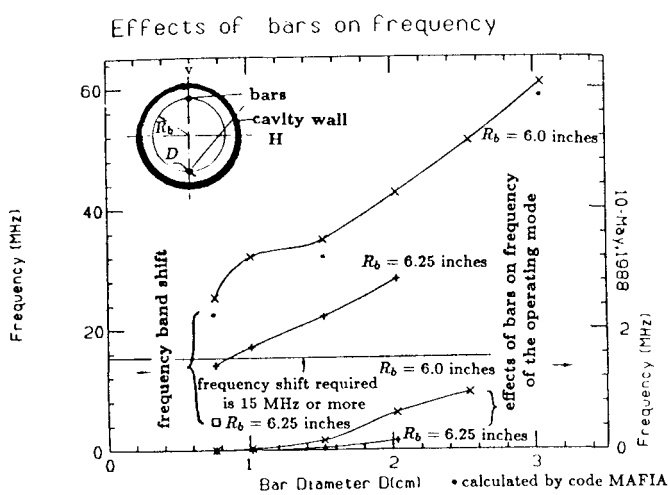

Figure 10 Frequency shift of unwanted mode vs diameter of bar pair in different radial location.

Future Plan

Based on the above experimental data, we are able to determine the real dimensions of both deflecting and coupling cells of APS for CEBAF's rf separator. An additional ongoing experiment will give us the relationship between sizes of coupling windows on the wall of an input cavity and the coupling coefficient of the external waveguide with the structure. We are planning to build an rf separator prototype in the near future to test our design and possibly to measure the bunch length in the injector area (electron energy $\approx$ 5 MeV).[11]

Acknowledgments

This work was supported by the U.S. Department of Energy under contract number DE-AC05-84ER40150.

The author wishes to express many thanks to Richard York, Joseph J. Bisognano, Byung Yunn, Geoffrey A. Krafft, David R. Douglas, and Christoph W. Leemann for helpful discussions, and to Brian Brooks and Timothy Mason for support work.

References

1. P. Bernard, et al., CERN 68-30, 1968.
2. G. A. Loew, et al., 5th Inter. Conf. on High Energy Acclerators, Frascati, 551 (1965).
3. O. H. Altenmueller, et al., Rev. Sci. Instr., 35, 438 (1964).
4. H. Hahn, H. J. Halama, Rev. Sci. Instr., 36, 1788 (1965).
5. H. Hahn, H. J. Halama, NIM, 45, 141 (1966).
6. C. G. Yao, CEBAF Design Handbook, 1987, section 6.9.
7. W. Bauer, H. Hahn, Particle Accelerators, 3, 193 (1972).
8. T. Kikuchi, et al., Japan. Jour. Appl. Phy., 9, No. 6, 679 (1970).
9. C. G. Yao, NIM, A240, 23 (1985).
10. B. C. Yunn, CEBAF-TN-0090, 1988.
11. R. C. York and C. G. Yao, CEBAF-TN-0089, 1988.